Vertical structure of the Venus cloud top from the VeRa and VIRTIS observations onboard Venus Express

Y.J. Lee [a,b,*], D.V. Titov [a,c], S. Tellmann [d], A. Piccialli [a], N. Ignatiev [e], M. Pätzold [d], B. Häusler [f], G. Piccioni [g], P. Drossart [h]

[a] Max Planck Institute for Solar System Research, 37191 Katlenburg-Lindau, Germany
[b] Institut für Geophysik und extraterrestrische Physik, Technische Universität Braunschweig, Braunschweig, Germany
[c] ESA/ESTEC, Noordwijk, The Netherlands
[d] Rhenish Institute for Environmental Research, Universität zu Köln, Cologne, Germany
[e] Space Research Institute (IKI), Moscow, Russia
[f] Universität des Bundeswehr, München, Germany
[g] IASF/INAF, Rome, Italy
[h] LESIA, Observatoire de Paris, Meudon, France

A R T I C L E   I N F O

A B S T R A C T

We investigate the Venus cloud top structure by joint analysis of the data from Visual and Thermal Infrared Imaging Spectrometer (VIRTIS) and the atmospheric temperature sounding by the Radio Science experiment (VeRa) onboard Venus Express. The cloud top altitude and aerosol scale height are derived by fitting VIRTIS spectra at 4–5 μm with temperature profiles taken from the VeRa radio occultation. Our study shows gradual descent of the cloud top from 67.2 ± 1.9 km in low latitudes to 62.8 ± 4.1 km at the pole and decrease of the aerosol scale height from 3.8 ± 1.6 km to 1.7 ± 2.4 km. These changes correlate with the mesospheric temperature field. In the cold collar and high latitudes the cloud top position remarkably coincides with the sharp minima in temperature inversions suggesting importance of radiative cooling in their maintenance. This behaviour is consistent with the earlier observations. Spectral trend of the cloud top altitude derived from a comparison with the earlier observations in 1.6–27 μm wavelength range is qualitatively consistent with sulphuric acid composition of the upper cloud and suggests that particle size increases from equator to pole.

© 2011 Elsevier Inc. All rights reserved.

1. Introduction

Venus is completely shrouded by a thick cloud deck. Imaging of the planet at different wavelengths from ultraviolet to thermal infrared shows plenty of morphological features originated from inhomogeneous distribution of absorbers and/or temperature at the cloud top. The cloud features show significant temporal and spatial variations suggesting changes in the cloud top structure. Tracking of the cloud markings is used to derive wind speed at the cloud level. Also the cloud tops are in direct radiative energy exchange with the Sun and space. Thus altitude, vertical structure and properties of the Venus cloud tops significantly affect chemistry, radiation and dynamics (Esposito et al., 2007). On the other hand this knowledge is crucially important for understanding of the cloud morphology, dynamics and radiative balance at these altitudes as well as for interpretation of remote sensing observations.

The cloud structure below ~60 km was investigated only in few locations by the Venera and Pioneer-Venus descent probes (Seiff, 1983; Esposito et al., 1983, 1997). Recent stellar and solar occultations onboard Venus Express sounded in detail the upper haze from 120 km to 70 km (Wilquet et al., 2009). The cloud top region (70–60 km) falls in the gap between descent probe and occultation observations and was only remotely studied.

Nadir remote sensing observations provide indirect information about the cloud top altitude, its variations over the planet and aerosol vertical structure. Thermal IR spectroscopy at 6.25–40 μm and 3–5 μm suggested vertical cloud scale heights from 3–4 km to 5.2 km in the equatorial region respectively (Zasova et al., 1993; Roos et al., 1993). Zasova et al. (1993) analyzed Venera-15 thermal emission spectra and found that the scale height varied from ⩽1 km to 5 km in the cold collar region. Limb observations by the Pioneer-Venus orbiter indicated decrease of the cloud top altitude with latitude (Lane and Opstbaum, 1983). Schofield and Taylor (1983) derived mean cloud top altitude at ~66.5 km for $\lambda \sim 10$ μm with a

trend to decrease with latitude. Zasova et al. (1993, 2007) confirmed the latitudinal decreasing trend of cloud top altitude from equator (~70 km) towards the pole (~60 km).

The Venus Express mission opened a new era in the Venus studies. Since the orbit insertion in April 2006 the spacecraft has been performing a remote sensing survey of Venus (Svedhem et al., 2009) delivering a wealth of new data about the cloud structure (Wilquet et al., 2009), morphology (Markiewicz et al., 2007; Titov et al., 2008, 2012; Piccioni et al., 2007), atmospheric temperatures (Grassi et al., 2008, 2010; Tellmann et al., 2008). Recently Ignatiev et al. (2009) used the near IR imaging spectroscopy by VIRTIS/Venus Express to map the cloud top altitude over the planet. He also found that the cloud top altitude decreased from ~74 km in the middle and low latitudes to ~63 km in pole regions.

In this paper we develop and carry out the joint analysis of the spectroscopic observations by VIRTIS and temperature structure measurements by VeRa to investigate the cloud top structure. This approach is applied for the first time and became possible due to the presence of both experiments onboard Venus Express.

2. Motivation and idea of the method

Two experiments onboard Venus Express sound remotely the Venus mesosphere and upper troposphere. Thermal emission spectroscopy in the region of 4.3 μm CO_2 band by VIRTIS allows one to retrieve vertical profiles of atmospheric temperature in the altitude range from 90 km to the cloud top (70–65 km) (Grassi et al., 2008, 2010). Radio-occultation sounding by the VeRa experiment penetrates deeper through the clouds and reaches the altitude of ~40 km (Tellmann et al., 2008). Comparison of the results of the two remote sensing techniques reveals systematic differences in derived temperature structure below 70 km (Fig. 1). Fig. 1 compares selected temperature profiles from two experiments for four local times and latitudinal zones. Below 70 km the VIRTIS temperatures are systematically lower than those derived by VeRa.

Explanation of this fact could be twofold. Firstly, the observations by two experiments are not simultaneous and co-located, so the difference can be due to temporal and spatial variations of the mesospheric temperature field. Secondly, the disagreement can be explained by that radio-occultation technique is not sensitive to the presence of clouds while thermal emission spectroscopy is. The retrieval of temperature profiles from VIRTIS spectra is based on an a priori assumption about aerosol structure and properties at the cloud tops (Grassi et al., 2008). Any uncertainties in the cloud model would affect the retrieved temperature profile. We note that, in general, thermal emission spectroscopy allows one to retrieve both temperature and aerosol structure in a self-consistent way. However this requires broad spectral range in which aerosol extinction varies significantly like was in the case of infrared Fourier spectrometer onboard Venera-15 (Zasova et al., 1993). VIRTIS covers only short part of the Venus thermal emission spectrum (3–5 μm) that does not enable distinguishing between temperature and aerosol effects on the emission spectra. Since the disagreement in the temperature structure derived from two experiments is systematic and correlates with the cloud, we conclude that the discrepancy is due to inaccuracy of the aerosol model assumed in the VIRTIS temperature retrievals.

The above discussed discrepancy motivated a development of a method of joint analysis to study the cloud top structure. The approach is based on that radio-occultation technique provides atmospheric temperature profiles independent of aerosol properties, while thermal emission spectra depend on both temperature and cloud structure. We use the radio-science temperature profiles and fit the VIRTIS spectra by tuning parameters of the cloud top model. Since VeRa and VIRTIS cannot perform simultaneous

observations, special attention was paid to selection of sub-sets of both observations in order to make them as close as possible in space and time.

3. Data set

3.1. Radio-occultation experiment by VeRa

VeRa sounds the Venus atmosphere by transmitting radio signals at 3.6 and 13 cm wavelengths in the Earth occultation seasons (Häusler et al., 2006; Pätzold et al., 2007). After propagating through the Venus atmosphere, the radio signal is recorded by the ground stations with the closed loop receiving technique. Measurements of the signal properties and their changes as a function of time together with accurate knowledge of the spacecraft orbit during occultation enable retrievals of vertical profiles of the atmospheric density, pressure, and temperature from ~40 to ~90 km altitude with vertical resolution of few hundred metres and accuracy better than fractions of a Kelvin in the very deep atmosphere (Tellmann et al., 2008). Bending of the radio beam in the Venus atmosphere and spacecraft motion during occultation result in ~50 km spatial averaging at the cloud top. Since the beginning of the orbital mission in April 2006 VeRa performed more than 175 Earth occultation experiments resulting in a data set of more than 350 atmospheric profiles. They provided good latitudinal coverage in the Southern hemisphere. In the Northern hemisphere occultations are mainly clustered at high latitudes. The data set covers roughly all local times.

For this study we selected a sub-set of 113 VeRa temperature profiles taken in orbits #254 (2006-12-31) through #986 (2009-01-01), and distributed them into 5° latitude bins (except 40S–46S, 46S–50S, 50S–56S, and 56S–60S bins, according to shapes of temperature profiles). Since mesospheric temperatures depend mainly on latitude (Seiff et al., 1983), we neglect local time dependence of the temperature field. This gives 3–8 VeRa observations in each bin. Our analysis is limited to the Southern hemisphere for two reasons: (1) VeRa coverage of Northern hemisphere, especially middle latitudes, is poor and (2) VIRTIS observations cover mainly Southern hemisphere. Fig. 2 shows individual and mean temperature profiles for each latitude bin indicating strong variations with latitude. Atmospheric temperature monotonically increases with depth in low latitudes (<45S). Middle and high latitudes up to ~80S are characterized by temperature profiles with strong and sharp inversions at 60–65 km. Poleward from 80S the temperature profiles are almost isothermal for 10–15 km above the tropopause that approximately coincides with the cloud tops.

3.2. Thermal emission spectroscopy by VIRTIS

VIRTIS is an imaging and high-resolution spectrometer with three channels VIRTIS-M-vis, VIRTIS-M-IR and VIRTIS-H (Drossart et al., 2007; Piccioni et al., 2008). The VIRTIS-M infrared channel covers spectral range from 1.84 μm to 5 μm. Thermal emission at 3–5 μm bears information about the cloud top structure. We used only night side observations with less than 0.36 s exposures to avoid contamination by reflected solar light and detector saturation. We sorted the selected spectra from the whole VIRTIS-M-IR data set, collected till 27 October, 2008 (orbit #921), in the same latitude bins as VeRa temperature profiles (Fig. 2). Within each latitude bin the spectra were also grouped according to the value of emission angle. The range of emission angle variations within each group was limited to ±0.1° around the mean value. In this study we assumed that VIRTIS spectra are independent of local solar time. Thus latitude and emission angle were two parameters used to group the spectra. The number of spectra within each latitude
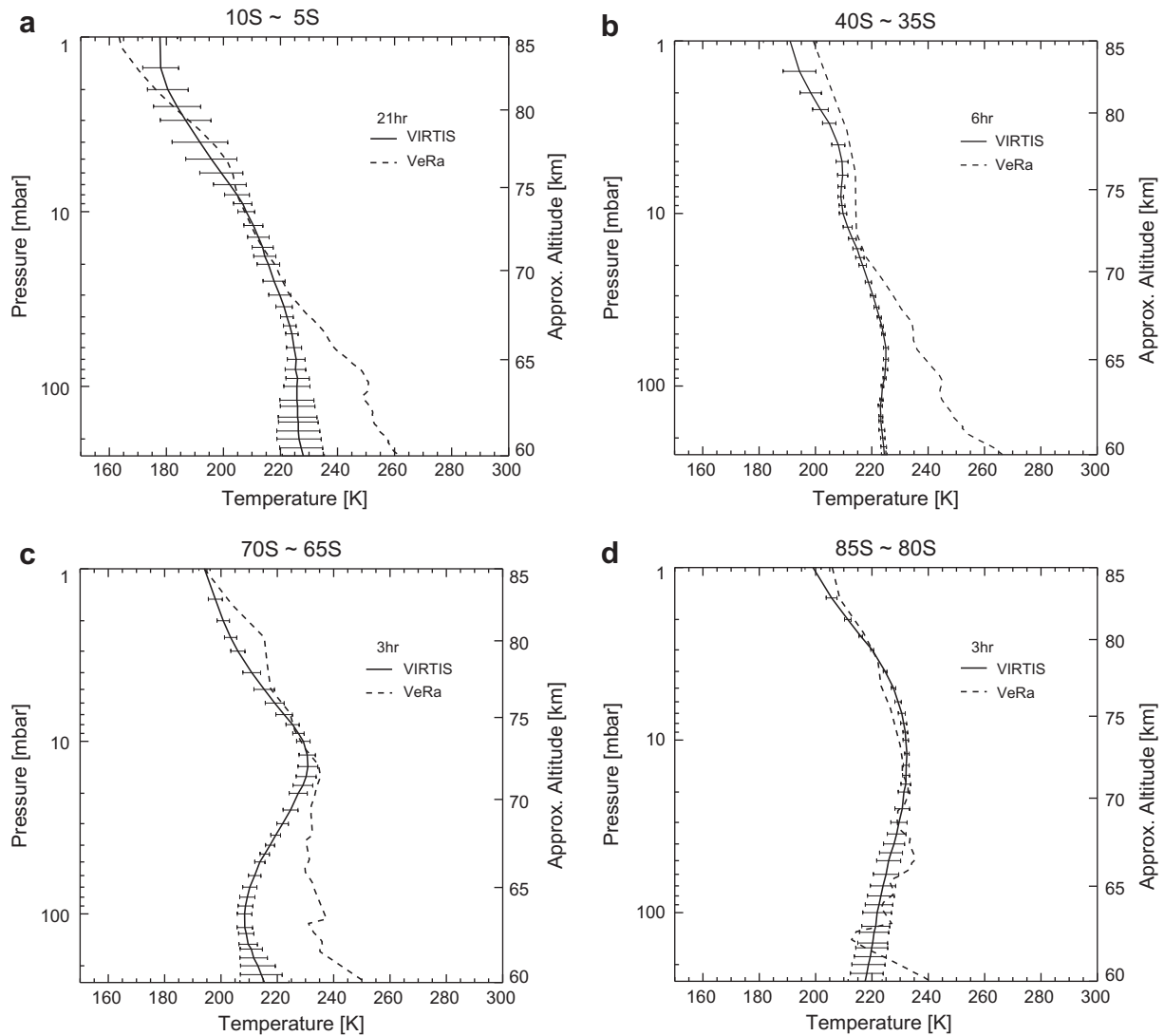
Fig. 1. Comparisons of temperature profiles derived from VIRTIS (solid line) and observed by VeRa (dashed line) experiments in same latitudinal bin and local time (shown in right upper corner of each figure). (a) Low latitude case with VIRTIS orbit #824_07 and VeRa orbit #927, (b) middle latitude case with VIRTIS #634_03 and VeRa #641, (c) cold collar case with VIRTIS #664_04 and VeRa #665 and (d) polar region with VIRTIS #664_04 and VeRa #662 data.

bin varies depending on the instrument footprint and ranges from 30 to 300. Each latitude bin contains from 13 to 31 groups of spectra with similar emission angle. Total number of VIRTIS spectra included in the analysis is 252.

Fig. 3 shows examples of the VIRTIS-M-IR spectra within selected latitude bins with pronounced features typical for Venus emission spectra. In Fig. 3a and b the CO_2 bands at 4.2–4.4 μm and 4.8–4.9 μm are clearly seen as absorption features indicating monotonic temperature profile. In the continuum outside of CO_2 bands (i.e. at ~4 μm, 4.6–4.7 μm, and ~5 μm) the spectrum is formed by emission from warm cloud tops, while inside the bands the spectrometer sees colder atmosphere above the clouds. Cold collar spectra show inversions in the "shoulders" of the 4.3 μm band at ~4.15 μm and ~4.5 μm, while the weaker 4.8 μm band appears "in emission" indicating temperature inversions right above the cloud tops (Fig. 3c). Almost constant brightness temperature in the spectral range from 4.5 μm to 5 μm in Fig. 3d suggests quasi-isothermal layer above the cloud tops. We note that the features in the VIRTIS spectra and their latitudinal changes (Fig. 3) are in qualitative agreement with temperature structure measured by VeRa (Fig. 2).

VIRTIS spectra show oscillations (for instance, at 4.5–4.6 μm in Fig. 3) caused by slightly different sensitivity of odd and even lines of the detector that remain even after radiometric calibration (Gilli et al., 2009). In this work we used only odd lines which show a more pronounced shape of the weak 4.8 μm CO_2 absorption band.

4. Method of the cloud top structure retrieval

In this work we retrieve the cloud top structure with ad-joint data sets from the VIRTIS and VeRa observation. We use the temperature profiles measured by the radio-science experiment VeRa which are not affected by aerosols and compare VIRTIS spectra with synthetic spectra for an exponential aerosol model. Then we derive parameters of the model by fitting VIRTIS thermal emission spectra using their sensitivity to the cloud top structure.

4.1. Model of the upper cloud

Venus cloud deck has complex vertical structure consisting of three layers each having different microphysical and optical
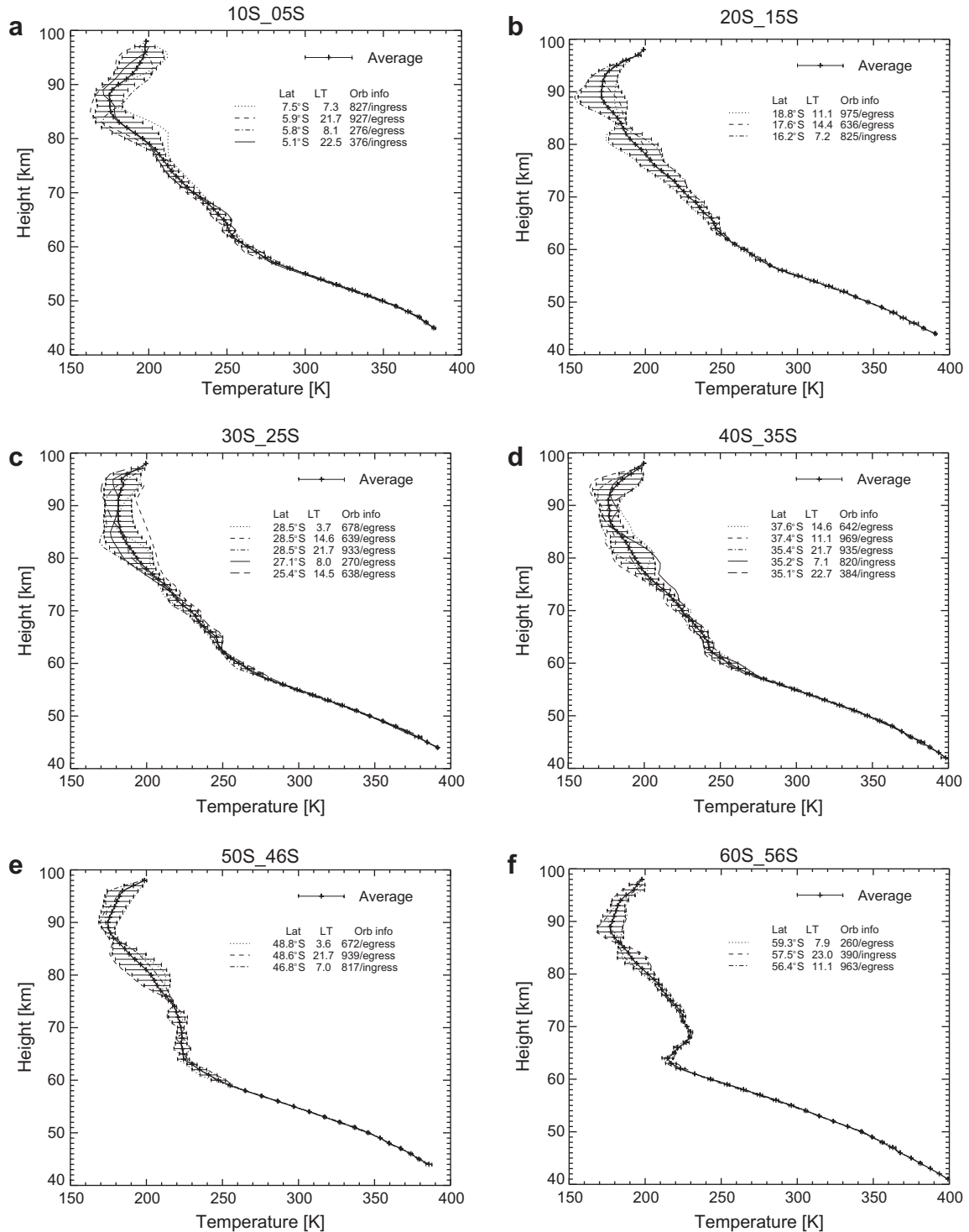
Fig. 2. VeRa temperature profiles for every second latitude bin (figures on the top of each sub-plot). Individual observations are shown with their legends in the upper right corner. Thick black line and horizontal bars show mean profile and standard deviation.

properties (Ragent et al., 1985; Esposito et al., 1997). The cloud also shows strong temporal and spatial variations. Since the outgoing thermal emission is formed mainly in the upper part of the cloud above ~60 km, we used a simplified cloud model. We assumed exponential volume extinction profile of aerosol above 60 km and constant extinction below this altitude:

$$E(z) = \begin{cases} E_0 e^{\left(\frac{z-65}{H}\right)}, & z > 60 \text{ km} \\ E(60), & z < 60 \text{ km} \end{cases} \tag{1}$$

where $E(z)$ is vertical profile of the volume extinction coefficient, H is aerosol scale height, E_0 is extinction at 65 km. We assume constant aerosol volume extinction in the 4.4–5.0 μm range and define the "cloud top altitude" as the height of the unit optical depth ($z_{\tau=1}$) level. Thus our cloud model has two parameters: cloud top altitude $z_{\tau=1}$ and aerosol scale height H. Fig. 4 shows examples of the vertical profiles of aerosol volume extinction coefficient.

The upper cloud is dominated by "mode 2" ($r \sim 1$ μm) particles (Pollack et al., 1980; Ragent et al., 1985). We used optical
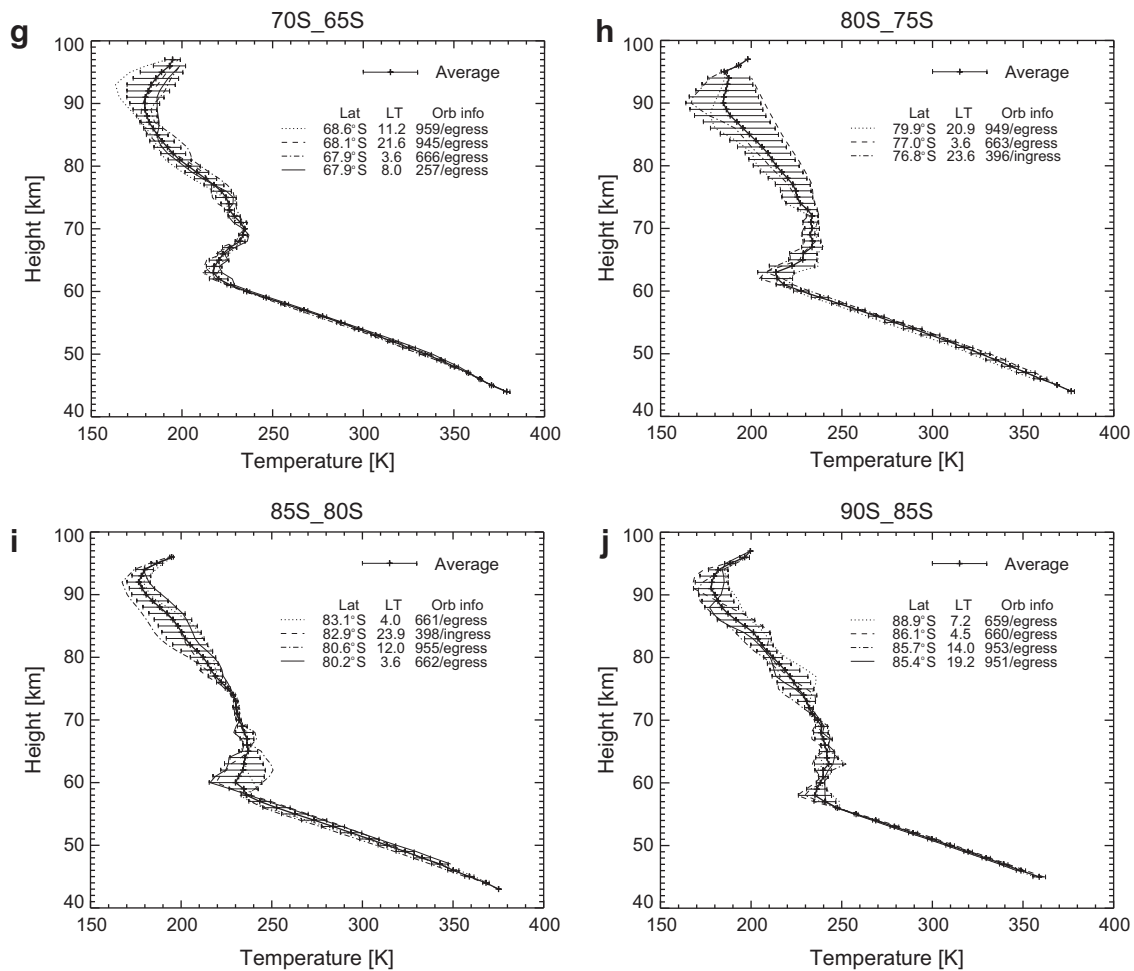
Fig. 2 (*continued*)

properties of the "mode 2" to calculate thermal emission spectra. Fig. 5 shows single scattering albedo and asymmetry factor for the Henyey–Greenstein phase function calculated for this model.

4.2. Radiative transfer model

Both thermal emission from the planet and scattered solar light contribute to the outgoing radiation in the 4.4–5.0 μm range. The latter is ignored since we use night side data only. The main sources of opacity are clouds, and CO_2 and CO gases. In this study we took into account the fundamental CO_2 absorption band at 4.3 μm, the weak CO_2 band at 4.8 μm and the CO band at 4.6 μm.

In order to take into account both fine structure of the gaseous absorption bands and multiple scattering in the cloud we merged the fast and accurate method of line-by-line calculations (Titov and Haus, 1997) with radiative transfer routine SHDOM (Spherical Harmonic Discrete Ordinate Method) (Evans, 1998). For each wavelength the combined algorithm had the following steps. First, vertical profile of gaseous absorption coefficient was calculated for the atmospheric model based on the VeRa temperature profile (Fig. 2). The spectral parameters were taken from the HITRAN 2008 database (Rothman et al., 2009). Temperature and pressure corrections were applied for both line intensity and self-broadened half-width. Sub-Lorentz line correction was taken from Winters et al. (1964). The line cut-off value was set to 200 cm^{-1}, and the wavenumber step was 0.1 cm^{-1}. Second, vertical profile of aerosol volume absorption coefficient was calculated for the selected cloud

model (Fig. 4). Then the sum of vertical profiles of monochromatic aerosol and gaseous extinction coefficients was used as input for SHDOM that returned intensity of the outgoing radiation at the selected wavelength. The above described procedure, repeated for all wavelengths in 4.3–5.0 μm range, yielded monochromatic spectrum of the Venus thermal emission. It was convolved with Gaussian function with full-width-half-maximum (FWHM) of 15 nm to get VIRTIS synthetic spectrum $I_{syn}(\lambda)$ (Ignatiev et al., 2009).

4.3. Sensitivity to the model parameters

A VIRTIS synthetic spectrum depends on the cloud top model. In this work we determine two model parameters – cloud top altitude $Z = Z_{\tau=1}$ and aerosol scale height H – by fitting the VIRTIS measurements in each latitude bin. Sensitivity of the synthetic spectra and, hence, accuracy of the parameter retrievals strongly depend on the temperature structure. Fig. 6 shows several typical situations encountered in our retrievals. At low latitudes characterized by monotonic temperature profile (Fig. 2a–e) the synthetic spectra significantly depend on the cloud top model (Fig. 6a and b). On the contrary, in the polar regions with almost isothermal atmosphere above the clouds (Fig. 2i and j) sensitivity to the aerosol structure is rather weak (Fig. 6c and d).

The strong dependence of synthetic spectra on the cloud model parameters (Fig. 6e and f) is also typical for the "cold collar" region with strong temperature inversions (Fig. 2f–h). However retrievals of the aerosol parameters are more complex here. Fitting of a
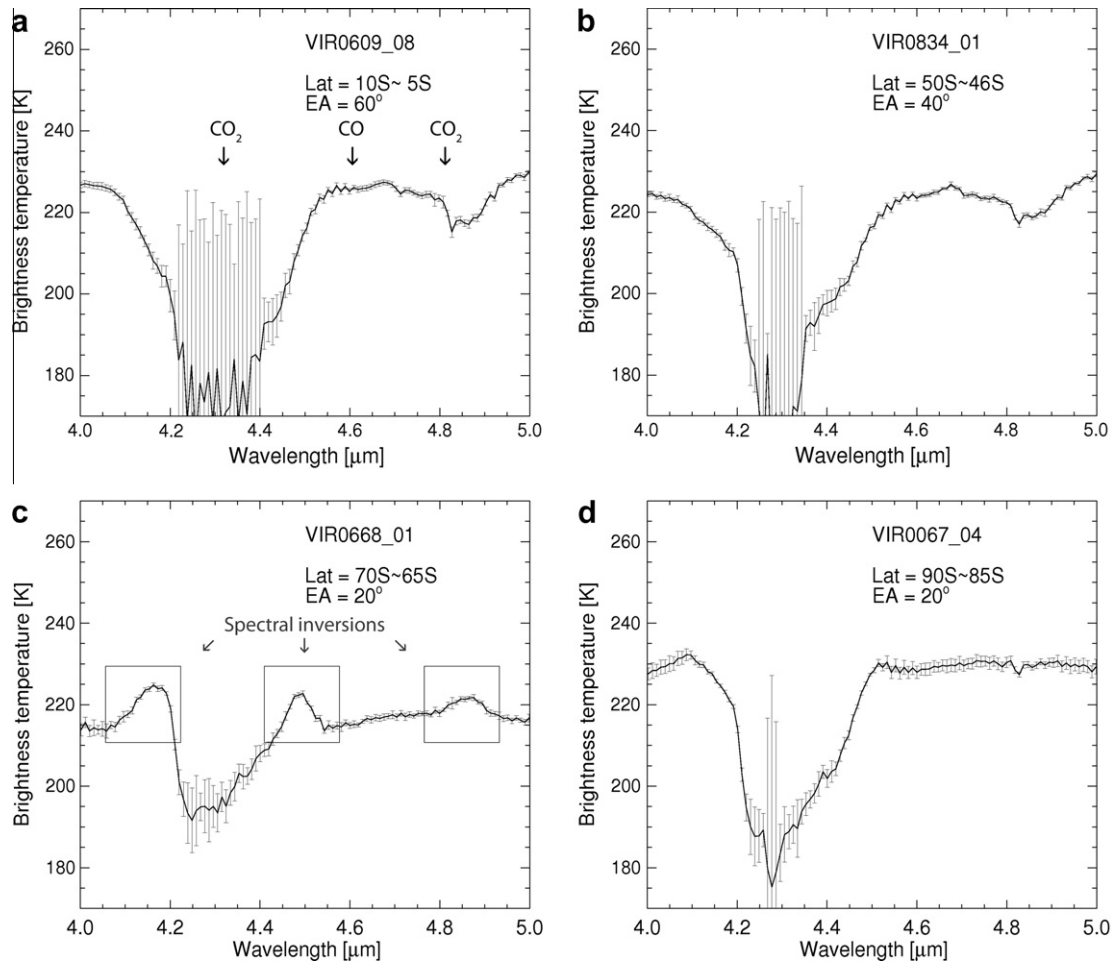
Fig. 3. Examples of the VIRTIS-M-IR brightness temperature spectra in the region of 4.3 μm CO_2 band. VIRTIS data files, latitude bin (Lat), and emission angle (EA) are given in the legends in the upper right corner of each sub-plot. Solid lines and bars represent mean spectra and standard deviations within the selected group. Positions of gaseous absorption bands and spectral inversions are shown in panels (a) and (c) correspondingly.
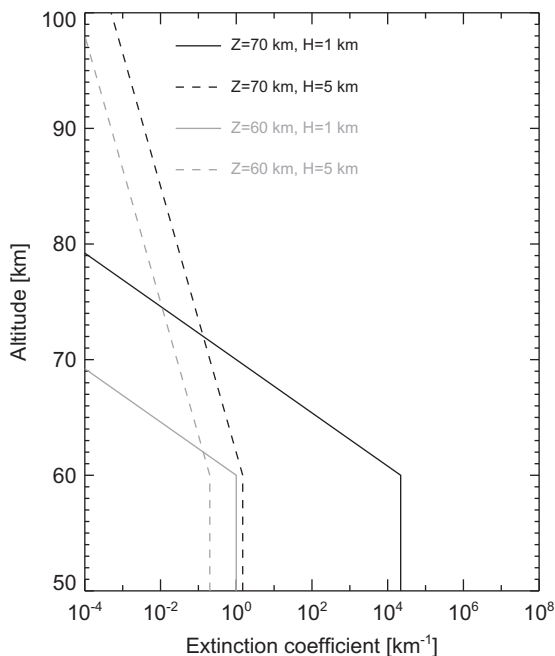
Fig. 4. Example of vertical profiles of aerosol volume extinction.
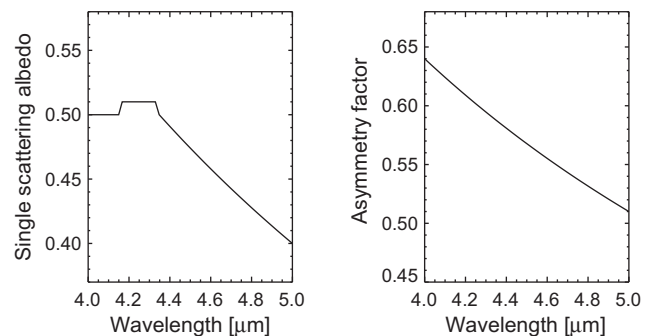
Fig. 5. Single scattering albedo and asymmetry parameter for mode 2 particles (Ragent et al., 1985).

VIRTIS spectrum is often ambiguous resulting in two almost equally good formal solutions: the first one having small aerosol scale height and low clouds and the second solution with large aerosol scale height and high clouds. Fig. 7 compares synthetic spectra for small and large values of the aerosol scale height. For $H = 1$ km the model with $Z = 63$ km fits well the observed VIRTIS spectrum (Fig. 7a). For $H = 6$ km synthetic spectra approach quite close to the VIRTIS measured spectrum, but still fail to reproduce its main feature – inversion in the shoulders of the 4.3 μm CO_2 band. This behaviour can be qualitatively explained by the following
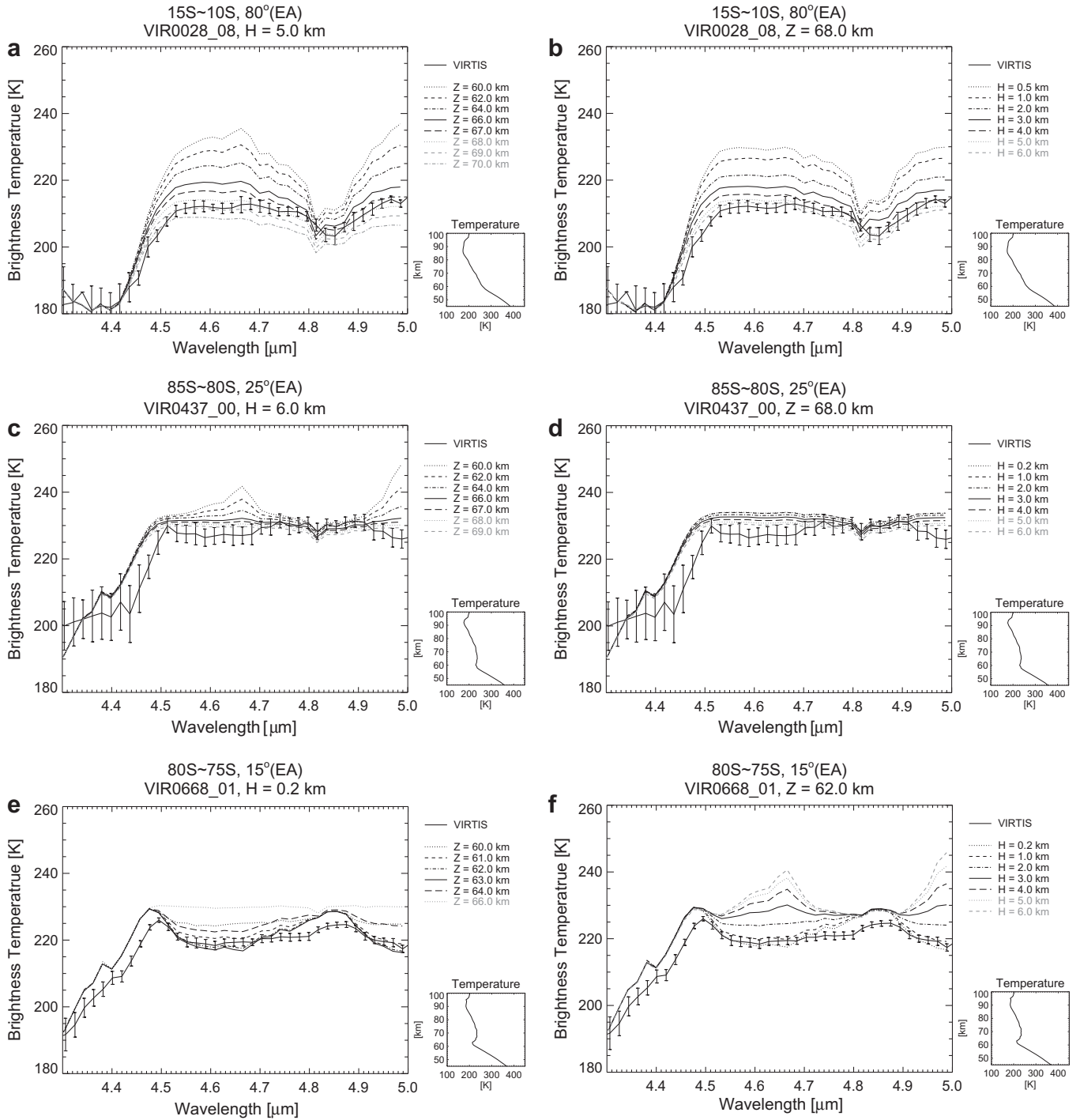
Fig. 6. Synthetic spectra and VIRTIS measurements: (a and b) low latitudes; (c and d) polar region; (e and f) "cold collar". In the left column (sub-panels a, c, e) the aerosol scale height H is fixed and the cloud top altitude Z is varied. In the right column (sub-panels b, d, f) H is varied and Z is fixed. The legends on the top of each sub-panel show latitude bin, emission angle (EA), VIRTIS data file, and values of constant H or Z. Solid line is VIRTIS spectrum and other lines correspond to different values of variable parameters (see legends in the upper right of each sub-panel). Temperature structure is shown in the lower right of each sub-panel.

consideration. The sharp cloud top placed right at the temperature minimum of inversion allows thermal emission to form in the pure gaseous atmosphere in the inversion region above the cloud top thus resulting in spectral inversion. When aerosol is distributed with large scale height it dominates opacity in the temperature inversion region and simply masks the temperature inversion. The ambiguity is discussed in more detail below.

4.4. Retrieval of the cloud structure

The discrepancy between a synthetic spectrum $I_{Syn}(Z,H)$ and an observed one I_{Obs} is defined as follows:

$$D(Z,H) = \frac{\left(\sum_i^N |I_{Obs,i} - I_{Syn,i}(Z,H)|^2\right)}{N} \tag{2}$$
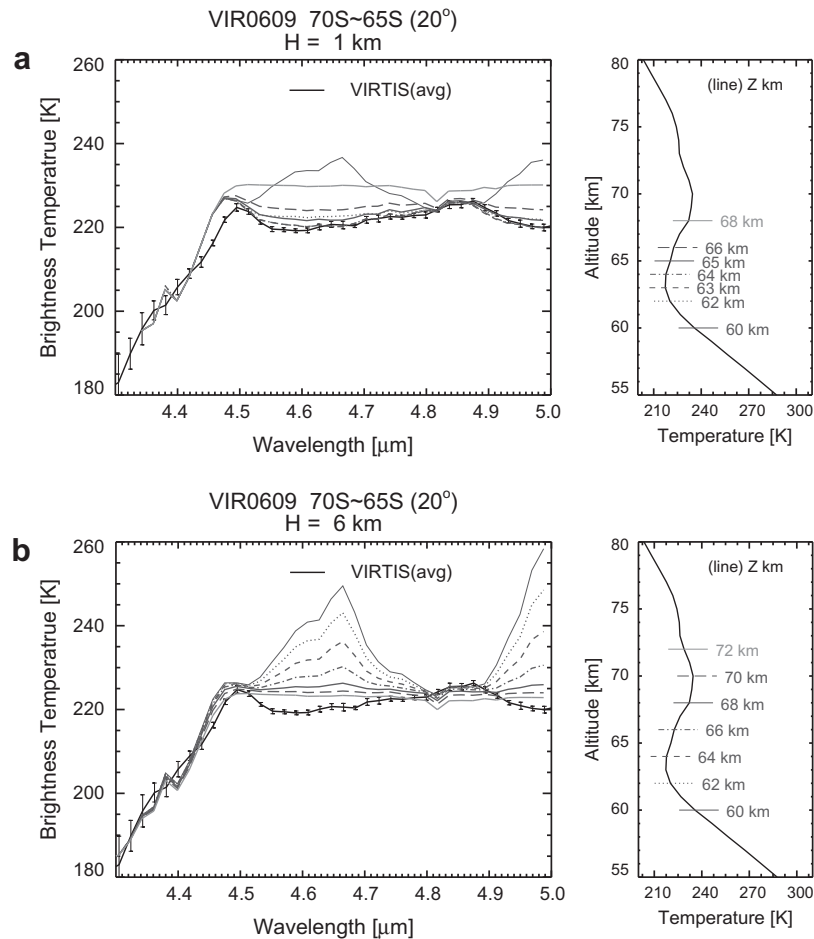
Fig. 7. Comparisons of synthetic spectra with VIRTIS observation in the "cold collar" region for small (a) and large (b) aerosol scale height. Left panels show brightness temperature spectra. Thick solid lines are VIRTIS spectra from the file VIR0609_00. Different grey lines are synthetic spectra for several cloud top altitudes shown on the right panels together with VeRa temperature profiles.

where N is the number of spectral points. Only the points in the continuum (4.4–4.8 μm and 4.9–5.0 μm) are included in the sum. The procedure of cloud model determination consisted of minimization of the discrepancy function $D(Z, H)$ in two-parameter space. $D(Z, H)$ was first calculated on a coarse grid with $\Delta Z = 2$ km and $\Delta H = 1$ km to find an approximate minimum of the discrepancy function. Then a fine grid with steps $\leqslant 1$ km was made by inverse parabolic interpolation around the approximate minimum to find its position more accurately (Press et al., 1992). We continued the process until grid size becomes less than 0.05 km. Fig. 8 shows typical examples of the two-dimensional discrepancy function $D(Z, H)$. In low latitudes, where air temperature monotonically increases with depth, the minimum of discrepancy function is well defined (Fig. 8a). The fact that isolines of D function are almost horizontal indicates that the cloud top altitude is better constrained than the scale height. Fig. 8b shows more difficult case of strong temperature inversion in the "cold collar" region. The discrepancy function can have two local minima: one for small (black dot) and one for large (grey dot) values of H. This illustrates the qualitative discussion in the previous subsection. In many cases we resolve this ambiguity by using qualitative arguments and giving priority to the pair of model parameters, small aerosol scale height and low cloud top altitude, that succeed to reproduce inversion in the wings of the 4.3 μm CO_2 band.

5. Results and discussion

We derived the parameters of the cloud top structure from the joint analysis of the selected VIRTIS spectra (see examples in Fig. 3) and corresponding VeRa temperature profiles for each latitude bin (Fig. 2) that provided complete coverage of the Southern hemisphere. Fig. 9 shows latitude dependence of the cloud parameters. In the low and middle latitudes the cloud top altitude is 67.2 ± 1.9 km. The aerosol scale height is 3.8 ± 1.6 km which is close to that of the gas. Poleward of $\sim$50S the cloud structure changes significantly. The cloud top height decreases with latitude and reaches minimum of $\sim$63 km in the polar region. Aerosol scale height also decreases to 1–2 km. Table 1 summarizes results of our analysis for three major latitudinal zones.

Table 1
Derived values of the cloud top structure for three latitudinal zones.

	Latitude range		
	Mid-low lat. (0S–56S)	Cold collar (56S–80S)	Polar region (80S–90S)
Aerosol scale height (km)	3.8 ± 1.6	2.1 ± 2.0	1.7 ± 2.4
Cloud top altitude (km)	67.2 ± 1.9	64.7 ± 3.2	62.8 ± 4.1
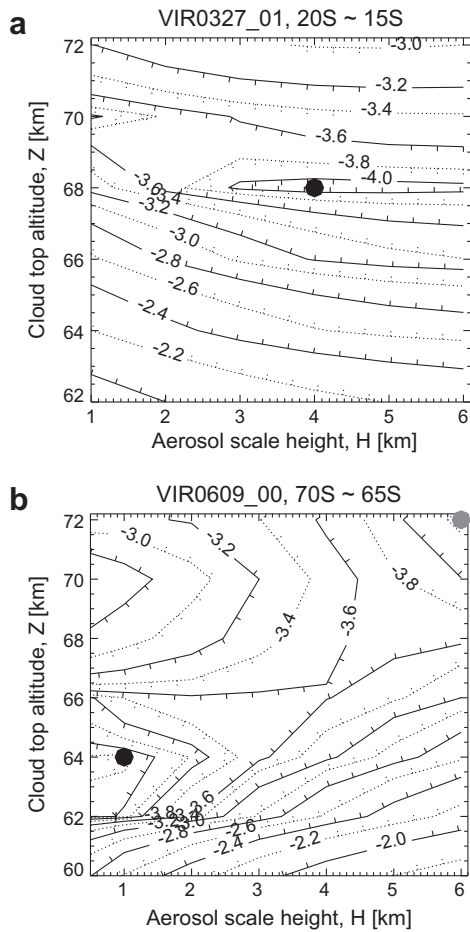
Fig. 8. Examples of two-dimensional fields of the discrepancy function $D(H, Z)$ in logarithmic scale for (a) low latitude and (b) "cold collar" cases. Big black dot marks the minimum and grey dot marks the secondary local minima. (a) Low latitude case (20S–15S) for VIRTIS data file VIR0327_01 and emission angle of 60°. (b) Cold collar case (70S–65S) for VIRTIS data file VIR0609_00 and emission angle 20°.
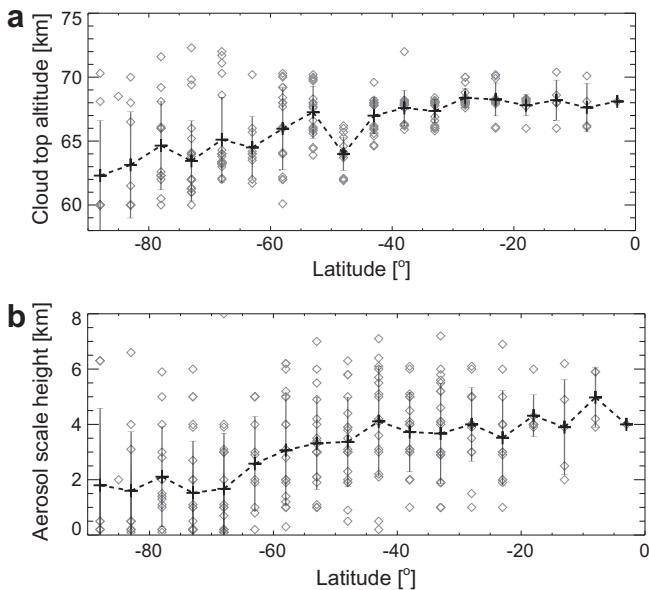
Fig. 9. Latitudinal distributions of the cloud top altitude (a) and cloud scale height (b). Black diamonds mark individual retrievals. Crosses and bars are mean values and standard deviations within each latitude bin.

We note again that the cold collar region is characterized by temperature inversions (Fig. 2f–h) that in some cases make the retrieval of the cloud structure ambiguous. However typical cold collar spectrum and especially spectral inversions in the wings of 4.3 μm CO_2 band can be only simulated with small aerosol scale height and low cloud top altitude (Figs. 6e, f and 7).

Fig. 10 compares latitude behaviour of the cloud top altitude derived in this work with results of the earlier observations. Our retrievals are consistent with the general trend for cloud top altitude to decrease with latitude, obtained earlier from the VIRTIS spectroscopy in the near-IR CO_2 bands (Ignatiev et al., 2009) and mid-IR spectroscopy by the Venera-15 Fourier spectrometer (Zasova et al., 2007). The cloud top altitude at 5 μm (diamonds) is around 3–6 km below the result at 1.6 μm (crosses) in all latitude. The tendency of the cloud top altitude to decrease with wavelength, shown in Fig. 10, is in quantitative agreement with that expected for sulphuric acid composition of the upper cloud at all latitudes (see Fig. 9 in Ignatiev et al., 2009). Our analysis also confirms the conclusions derived from the Venera-15 data that the aerosol scale height decreases towards the pole (Zasova et al., 1993, 2007), although 1.6 μm cloud top assumed the aerosol scale height of 4 km (Ignatiev et al., 2009).

Fig. 10 also shows two peculiarities. Firstly, the cloud top strongly descends from equator to pole in the wavelengths range 1–8 μm that sounds the upper cloud ($Z_{\tau=1} > 57$ km), while there is almost no decrease in cloud top altitude at 27.4 μm (open circles) that probes the middle cloud. This suggests that the upper cloud shrinks in vertical direction towards the pole while the middle cloud does not change its altitude.

The second peculiarity seen in Fig. 10 is that poleward from the cold collar the 8 μm cloud top (filled circles) is located deeper than that at 5 μm while the trend is opposite in low latitudes. This tentatively indicates differences in particle sizes at low and high latitudes. Spectral behaviour of aerosol extinction efficiency depends on particle size. For standard microphysical model of the Venus clouds the extinction efficiency for modes 2 and 2' ($r_0 = 1$–1.4 μm) at 8.2 μm exceeds that at 5 μm (see Fig. 15 in Zasova et al., 2007), meaning that in such a cloud the $\tau = 1$ level at 8.2 μm will be higher than that at 5 μm. This is what we see in Fig. 10 at latitudes below 50–60°. For larger particles with $r_0 = 3.85$ μm (mode 3, curve 4 in Fig. 15 from Zasova et al., 2007) the ratio of extinction efficiencies is reversed resulting in that the cloud top at 8 μm is deeper that at 5 μm. This is exactly what Fig. 10 shows in the polar regions. Thus, this comparison suggests an increase of particle size in the upper cloud from equator to pole. This conclusion is consistent with the analysis of night side
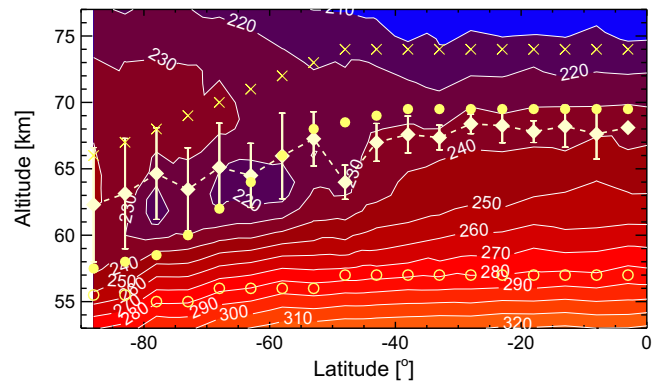
Fig. 10. Latitude dependence of the cloud top altitude overplotted on the VeRa latitude–altitude temperature field: diamonds – this study (4–5 μm); crosses – VIRTIS spectroscopy in the 1.6 μm CO_2 band (Ignatiev et al., 2009); filled and open circles – approximate Venera-15 Fourier spectroscopy in the 8.2 and 27.4 μm, respectively (Zasova et al., 2007).
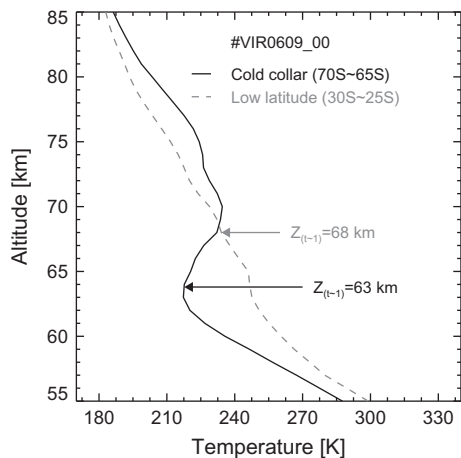
Fig. 11. Comparison of different latitudinal zone cloud top altitudes related with temperature profiles. VIRTIS orbit, latitudinal bin, cloud top altitude information are shown in figure. Cold collar case (black solid line) shows cloud top altitude below the temperature inversion layer, 63 km, and low latitude case (grey dashed line) shows high cloud top altitude, 68 km.

emissions observed by VIRTIS/Venus Express (Wilson et al., 2008), although they are believed to sound deeper into the cloud (50–55 km). We note however that the above derived conclusions from comparison of observations by different missions are based on the assumption that the Venus cloud structure mainly depends on latitude.

The changes in the cloud top structure are correlated with the mesospheric temperature field (Fig. 10). The cloud top starts descending at the outer edge of the "cold collar" ($\sim$50S) and approximately follows 230 K isoline. It is accompanied by decrease of the aerosol scale height. Drastic changes in the morphology of UV clouds, i.e. transition from the patchy and mottled clouds in low latitudes to bright uniform polar hood also occurs at this latitude (Markiewicz et al., 2007; Titov et al., 2008, 2012). This behaviour is likely of dynamical origin and is related to the Hadley circulation that has upwelling branch at equator and downwelling motions at $\sim$60°S (Svedhem et al., 2007).

The upper cloud has a very particular structure in the cold collar region. The very sharp cloud top with small aerosol scale height ($H \leqslant 1$ km) coincides with the temperature minima in the inversions (Fig. 11). This feature is likely of radiative origin. The sharp cloud top boundary provides effective cooling to space that maintains low temperatures. This mechanism is similar to that of formation of the temperature inversions at the Martian surface at night (Zurek et al., 1992). The inversions in turn create convectively stable conditions above the cloud top that prevents vertical mixing of aerosols and maintains sharp cloud boundary. This negative feedback between dynamical conditions and radiative effects makes the cold collar stable. The middle latitudes are also characterized by vanishing vertical wind sheer (Sánchez-Lavega et al., 2008) that suppresses wind sheer instabilities. Titov et al. (2008) used the peculiarities of stability distribution at the cloud top to qualitatively explain the global pattern of the UV markings.

The Venus Express payload has a great potential for the study of the structure and morphology of the Venus upper cloud and haze. Several directions of the work can be recommended for the future. The approach developed and proved in this work can be further applied to the VeRa data in combination with the VIRTIS-H spectroscopy. Although VIRTIS-H provides only "spot" measurements, it has regular coverage of both hemispheres, so that the method can be extended to the entire planet. Also VIRTIS-H measurements have a better chance to resolve retrieval ambiguities due to the higher spectral resolution. Solar and stellar occultations by

SPICAV/SOIR also provide excellent opportunity to study the upper haze structure. Although these observations sound a bit higher altitudes ($\sim$80 km), they can complement to the retrievals of the cloud top structure presented here. Finally limb imaging by VMC (Titov et al., 2012) and VIRTIS–vis can provide an important insight in the upper cloud structure and its latitudinal variability.

Acknowledgment

References

Drossart, P. et al., 2007. Scientific goals for the observation of Venus by VIRTIS on ESA/Venus Express mission. Planet. Space Sci. 55, 1653–1672.

Esposito, L.W., Knollenberg, R.G., Marov, M.V., Toon, O.B., Turco, R.P., 1983. The clouds and hazes of Venus. In: Hunten, D.M., Colin, L., Donahue, T.M., Moroz, V.I. (Eds.), Venus. University of Arizona Press, Tucson, AZ, pp. 484–564.

Esposito, L.W., Bertaux, J.-L., Krasnopolsky, V.A., Moroz, V.I., Zasova, L.V., 1997. Chemistry of lower atmosphere and clouds. In: Bougher, S.W., Hunten, D.M., Phillips, R.J. (Eds.), Venus II. University of Arizona Press, Tucson, AZ, pp. 415–458.

Esposito, L.W., Stofan, E.R., Cravens, T.E., 2007. Exploring Venus: Major scientific issues and directions. In: Esposito, L.W., Stofan, E.R., Cravens, T.E. (Eds.), Exploring Venus as a terrestrial planet. American Geophysical Union, Washington, DC, pp. 1–6.

Evans, K.F., 1998. The spherical harmonics discrete ordinate method for three-dimensional atmospheric radiative transfer. J. Atmos. Sci. 55, 429–446.

Gilli, G., López-Valverde, M.A., Drossart, P., Piccioni, G., Erard, S., Cardesín Moinelo, A., 2009. Limb observations of CO_2 and CO non-LTE emissions in the Venus atmosphere by VIRTIS/Venus Express. J. Geophys. Res. 114. doi:10.1029/2008JE003112.E00B29.

Grassi, D. et al., 2008. Retrieval of air temperature profiles in the venusian mesosphere from VIRTIS-M data: Description and validation of algorithms. J. Geophys. Res. 113. doi:10.1029/2008JE003075.E00B09.

Grassi, D. et al., 2010. Thermal structure of venusian nighttime mesosphere as observed by VIRTIS–Venus Express. J. Geophys. Res. 115. doi:10.1029/2009JE003553.E09007.

Häusler, B. et al., 2006. Radio science investigations by VeRa on board the Venus Express spacecraft. Planet. Space Sci. 54, 1315–1335. doi:10.1016/j.pss.2006.04.032.

Ignatiev, N.I., 2009. Altimetry of the Venus cloud tops from the Venus Express observations. J. Geophys. Res. 114. doi:10.1029/2008JE003320.E00B43.

Lane, W.A., Opstbaum, R., 1983. High altitude Venus haze from Pioneer Venus limb scans. Icarus 54, 48–58.

Markiewicz, W.J. et al., 2007. Morphology and dynamics of the upper cloud layer of Venus. Nature 450 (7170), 633–636. doi:10.1038/nature06320.

Pätzold, M. et al., 2007. The structure of Venus' middle atmosphere and ionosphere. Nature 450, 657–660.

Piccioni, G. et al., 2007. South-polar features on Venus similar to those near the north pole. Nature 450, 637–640.

Piccioni, G. et al., 2008. VIRTIS: The Visible and Infrared Thermal Imaging Spectrometer. ESA Special Publication, SP-1295. ESA Publication Division, Noordwijk, pp. 1–27.

Pollack, J.B. et al., 1980. Distribution and source of the UV absorption in Venus' atmosphere. J. Geophys. Res. 85, 8141–8150.

Press, W.H., Flannery, B.P., Teukolsky, S.A., Vetterling, W.T., 1992. Numerical Recipes in FORTRAN, second ed. Cambridge University, New York.

Ragent, B., Esposito, L.W., Tomasko, M.G., Marov, M. Ya., Shari, V.P., Lebedev, V.N., 1985. Particulate matter in the Venus atmosphere. Adv. Space Res. 5, 11, 85–115.

Roos, M. et al., 1993. The upper clouds of Venus: Determination of the scale height from NIMS/Galileo infrared data. Planet. Space Sci. 41, 505–514.

Rothman, L.S. et al., 2009. The HITRAN 2008 molecular spectroscopic database. J. Quant. Spectrosc. Radiat. Transf. 110, 533–572. doi:10.1016/j.jqsrt.2009.02.013.

Sánchez-Lavega, A. et al., 2008. Variable winds on Venus mapped in three dimensions. Geophys. Res. Lett. 35. doi:10.1029/2008GL033817.L13204.

Schofield, J.T., Taylor, F.W., 1983. Measurements of the mean, solar-fixed temperature and cloud structure of the middle atmosphere of Venus. Q. J. R. Meteorol. Soc. 109, 57–80.

Seiff, A., 1983. Thermal structure of the atmosphere of Venus. In: Hunten, D.M., Colin, L., Donahue, T.M., Moroz, V.I. (Eds.), Venus. University of Arizona Press, Tucson, AN, pp. 215–279.

Svedhem, H., Titov, D.V., Taylor, F.W., Witasse, O., 2007. Venus as a more Earth-like planet. Nature 450, 629–632.

Svedhem, H., Titov, D.V., Taylor, F.W., Witasse, O., 2009. The Venus Express mission. J. Geophys. Res. 114. doi:10.1029/2008JE003290.E00B33.

Tellmann, S., Pätzold, M., Häusler, B., Bird, M.K., Tyler, G.L., 2008. The structure of the Venus neutral atmosphere as observed by radio science experiment VeRa on Venus Express. J. Geophys. Res. 114. doi:10.1029/2008JE003204.E00B36.

Titov, D.V., Haus, R., 1997. A fast and accurate method of calculation of gaseous transmission functions in planetary atmospheres. Planet. Space Sci. 45 (3), 369–377.

Titov, D.V. et al., 2008. Atmospheric structure and dynamics as the cause of ultraviolet marking in the clouds of Venus. Nature 456, 620–623.

Titov, D.V. et al., 2012. Morphology of the cloud tops as observed by the Venus Express Monitoring Camera. Icarus 217 (2), 682–701.

Wilson, C.F. et al., 2008. Evidence for anomalous cloud particles at the poles of Venus. J. Geophys. Res. 113. doi:10.1029/2008JE003108.E00B13.

Wilquet, V. et al., 2009. Preliminary characterization of the upper haze by SPICAV/SOIR solar occultation in UV to mid-IR onboard Venus Express. J. Geophys. Res. 114. doi:10.1029/2008JE003186.E00B42.

Winters, B.H., Silvermans, S., Benedicts, W.S., 1964. Line shape in the wing beyond the band head of the 4.3 μm band of CO_2. J. Quant. Spectrosc. Radiat. Trans. 4, 527–537.

Zasova, L.V., Moroz, V.I., Esposito, L.W., Na, C.Y., 1993. SO_2 in the middle atmosphere of Venus: IR measurements from VENERA-15 and comparison to UV data. Icarus 105, 92–109.

Zasova, L.V., Ignatiev, N., Khatuntsev, I., Linkin, V., 2007. Structure of the Venus atmosphere. Planet. Space Sci. 55, 1712–1728. doi:10.1016/j.pss.2007.01.011.

Zurek, R.W., Barnes, J.R., Haberle, R.M., Pollack, J.B., Tillman, J.E., Leovy, C.B., 1992. Dynamics of the atmosphere of Mars. In: Keiffer, H.H., Jakosky, B.M., Snyder, C.W., Matthews, M.S. (Eds.), Mars. University of Arizona Press, Tucson, AN, pp. 835–933.